Nonlinear model reduction for dynamic analysis of cell population models

Yongchun Zhang[a], Michael A. Henson[b,*], Yannis G. Kevrekidis[c]

[a]*Department of Chemical Engineering, University of California, Santa Barbara, CA 93106, USA*
[b]*Department of Chemical Engineering, University of Massachusetts, Amherst, MA 01003-3110, USA*
[c]*Department of Chemical Engineering, Princeton University, Princeton, NJ 08544, USA*

Abstract

Transient cell population balance models consist of nonlinear partial differential-integro equations. An accurate discretized approximation typically requires a large number of nonlinear ordinary differential equations that are not well suited for dynamic analysis and model based controller design. In this paper, proper orthogonal decomposition (also known as the method of empirical orthogonal eigenfunctions and Karhunen Loéve expansion) is used to construct nonlinear reduced-order models from spatiotemporal data sets obtained via simulations of an accurate discretized yeast cell population model. The short-term and long-term behavior of the reduced-order models are evaluated by comparison to the full-order model. Dynamic simulation and bifurcation analysis results demonstrate that reduced-order models with a comparatively small number of differential equations yield accurate predictions over a wide range of operating conditions.
© 2002 Elsevier Science Ltd. All rights reserved.

1. Introduction

Many investigators have shown that continuous cultures of the microorganism *Saccharomyces cerevisiae* (baker's yeast) exhibit sustained oscillations in glucose limited environments under aerobic growth conditions (Parulekar, Semones, Rolf, Lievense, & Lim, 1986; Porro, Martegani, Ranzi, & Alberghina, 1988; Strassle, Sonnleitner, & Fiechter, 1989; von Meyenburg, 1973). Recent work in our group has demonstrated that the oscillatory dynamics can be captured by unstructured cell population models in which each cell is distinguished according to its mass (Mhaskar, Henson, & Hjortso, 2002; Zhu, Zamamiri, Henson, & Hjortso, 2000). The cell population model consists of a coupled set of nonlinear integro-partial differential equations. Discretization in the mass domain yields an approximate model with a large number of nonlinear ordinary differential equations. For our most recent model (Mhaskar et al., 2002) an accurate approximation consisting of 117 differential equations can be derived using orthogonal collocation on finite elements. Such high dimensional models are

not well suited for nonlinear dynamic analysis and controller design. Furthermore, structured cell population models derived from flow cytometric measurements may be completely intractable due to their significantly increased complexity (Srienc & Dien, 1992). Consequently, there is considerable motivation to develop reduced-order models that capture the key features of cell population dynamics.

After fast initial transients the dynamics of many distributed parameter systems evolve in a much lower dimensional space than the order of an accurate discretized model. This suggests that a reduced order model can be derived by projecting the dynamics of the high-order discretized model onto an appropriate reduced dimensional subspace. The development of mathematically rigorous order reduction techniques for nonlinear partial differential equation models such as the yeast cell population model is an open problem. However, several semi-empirical order reduction methods including proper orthogonal decomposition (POD) (Holmes, Lumley, & Berkooz, 1997) and approximate inertial manifolds (Foias, Sell, & Temam, 1988; Jolly, Kevrekidis, & Titi, 1990) can be used to construct a reduced dimensional space where the relevant dynamics evolve. In the POD approach, nonlinear model reduction is viewed as the problem of generating a convenient and in some sense optimal eigenfunction basis from which the reduced order model can

---

* Corresponding author.
  E-mail address: henson@ecs.umass.edu (M. A. Henson).

be constructed. The basis functions of the reduced dimensional space are generated empirically by applying principal component analysis (PCA) to spatiotemporal data generated from open-loop simulation of the full-order discretized model. Galerkin projection of the full-order model onto the empirical eigenfunctions yields the reduced-order nonlinear model.

In this paper, we apply the POD-Galerkin method to a discretized model of yeast cell population dynamics to derive reduced-order nonlinear models that are more amenable to dynamic analysis and controller design. Several issues associated with the collection of a representative simulation data set that are critical for construction of a useful reduced-order model are illustrated. This requires a methodology for evaluating the accuracy of the reduced-order model with respect to the full-order discretized model. Dynamic simulation is used to assess the short-term accuracy of reduced-order models generated from different spatiotemporal data sets. While open-loop simulation is an invaluable tool for such comparisons, we demonstrate that bifurcation analysis allows a more complete characterization of the reduced-order model dynamics. Our previous work has demonstrated that the yeast cell population model possesses a bifurcation structure where two critical values of the dilution rate separate regions of stable steady state and stable periodic solutions (Zhang, Zamamiri, Henson, & Hjortso, 2002). The long-term behavior of the reduced-order models is evaluated by comparing bifurcation diagrams of the full-order and reduced-order models. We show that a reasonably small number of empirical eigenfunctions is required to capture the long-term dynamic behavior of the full-order model.

The remainder of the paper is organized as follows. The yeast cell population model chosen for study is described in Section 2. The computational techniques used for nonlinear model reduction and bifurcation analysis are discussed in Section 3. The results of the model reduction study are presented and discussed in Section 4. A summary and conclusions are presented in Section 5.

2. Yeast cell population model

The dynamic model chosen for investigation consists of a segregated description of the cell population and a structured description of the growth medium. The resulting model is not a substitute for segregated yeast models that include a detailed description of the intracellular reactions. However, the structured medium description allows the model predictions to be compared with easily measured extracellular variables. Below the transient equations governing the cell population and the extracellular environment are presented. Our previous work (Mhaskar et al., 2002; Zhu et al., 2000) should be consulted for additional details.

Cell division in the budding yeast cell cycle is asymmetric. The smaller of the newborn cells obtained after division is referred to as a daughter cell while the larger cell is called

a mother cell. Newborn daughter cells must grow to attain the size of a newborn mother cell (characterized here by the cell transition mass) before starting a budding cycle. By contrast, newborn mother cells bud shortly after being born. After budding has occurred, the bud grows while the mass of the mother cell remains essentially constant. The bud grows until the cell attains the size necessary for division (characterized by the cell division mass).

A population balance equation (PBE) that describes the evolution of the cell mass distribution is formulated as follows (Eakman, Fredrickson, & Tsuchiya, 1966):

$$
\frac{\partial W(m,t)}{\partial t} + \frac{\partial [K(S')W(m,t)]}{\partial m}
$$
$$
= \int_0^\infty 2\,p(m,m')\Gamma(m',S')W(m',t)\,\mathrm{d}m'
$$
$$
- [D + \Gamma(m)]W(m,t), \tag{1}
$$

where m is the cell mass, $W(m,t)$ is the cell number density, $K(S')$ is the overall single cell growth rate, $S' = G' + E'$ is the effective substrate concentration (defined below), $p(m,m')$ is the newborn cell probability function, $\Gamma(m,S')$ is the division intensity function, and D is the dilution rate. The division intensity function is modeled as

$$
\Gamma(m,S') = \begin{cases} 0 & m \leqslant m_t^* + m_o \\ \gamma \mathrm{e}^{-\varepsilon(m-m_d^*)^2} & m \in [m_t^* + m_o, m_d^*] \\ \gamma & m \geqslant m_d^*, \end{cases} \tag{2}
$$

where m_t^* is the cell transition mass, m_o is the additional mass that mother cells must gain before division is possible, m_d^* is the cell division mass, and ε and γ are constant parameters. The newborn cell probability function has the form:

$$
p(m,m') = A \exp[-\beta(m - m_t^*)^2]
$$
$$
+ A \exp[-\beta(m - m' + m_t^*)^2] \tag{3}
$$

when $m < m'$ and $m' > m_t^* + m_o$; the function is identically zero otherwise. Here A and β are constant parameters. This function yields two Gaussian peaks in the cell number distribution, one centered at m_t^* corresponding to mother cells and one centered at $m_t^* - m'$ corresponding to daughter cells.
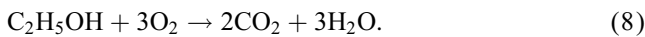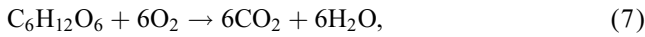
Functions (2) and (3) introduce dispersive effects into the PBE model that tend to counteract cell cycle synchrony (Porro et al., 1988) and dampen oscillatory dynamics. Sustained oscillations are obtained by modeling the dependence of the transition and division masses on the extracellular environment. The following saturation functions are used:

$$
m_t^*(S') = \begin{cases} m_{t0} + K_t(S_l - S_h) & S' < S_l \\ m_{t0} + K_t(S' - S_h) & S' \in [S_l, S_h] \\ m_{t0} & S' > S_h, \end{cases} \tag{4}
$$

$$m_d^*(S') = \begin{cases} m_{d0} + K_d(S_l - S_h) & S' < S_l \\ m_{d0} + K_d(S' - S_h) & S' \in [S_l, S_h] \\ m_{d0} & S' > S_h, \end{cases} \quad (5)$$

where S_l, S_h, m_{t0}, m_{d0}, K_t and K_d are constants.

The structured medium model allows both glucose and ethanol to serve as substrates for cell growth. The following reaction sequence accounts for the three major metabolic pathways: glucose fermentation, glucose oxidation and ethanol oxidation:

$$C_6H_{12}O_6 \rightarrow 2C_2H_5OH + 2CO_2, \quad (6)$$

$$C_6H_{12}O_6 + 6O_2 \rightarrow 6CO_2 + 6H_2O, \quad (7)$$

$$C_2H_5OH + 3O_2 \rightarrow 2CO_2 + 3H_2O. \quad (8)$$

The substrate balance equations are

$$\frac{dG}{dt} = D(G_f - G) \\ - \int_0^\infty \left[\frac{K_{gf}(G')}{Y_{gf}} + \frac{K_{go}(G')}{Y_{go}} \right] W(m,t)\, dm, \quad (9)$$

$$\frac{dE}{dt} = D(E_f - E) + \frac{92}{180} \int_0^\infty f(m) \frac{K_{gf}(G')}{Y_{gf}} W(m,t)\, dm \\ - \int_0^\infty \frac{K_{eo}(E')}{Y_{eo}} W(m,t)\, dm, \quad (10)$$

where G and E are the glucose and ethanol concentrations, respectively; G' and E' are the effective glucose and ethanol concentrations, respectively; G_f and E_f are the feed glucose and ethanol concentrations, respectively; Y_{gf}, Y_{go} and Y_{eo} are constant yield coefficients; and the ratio $\frac{92}{180}$ represents the mass of ethanol produced per mass of glucose consumed in Eq. (6). The effective substrate concentrations model the lagged response of cell metabolism to changes in the extracellular environment:

$$\frac{dG'}{dt} = \alpha_g(G - G'), \quad (11)$$

$$\frac{dE'}{dt} = \alpha_e(E - E'), \quad (12)$$

where α_g and α_e are constants.

The glucose fermentation rate K_{gf} is assumed to follow Monod kinetics with respect to glucose. The glucose oxidation rate K_{go} and ethanol oxidation rate K_{eo} are assumed to follow Monod kinetics with respect to both the substrate and the dissolved oxygen. Furthermore, the ethanol oxidation rate is assumed to be inhibited by glucose. The rate expressions are

$$K_{gf}(G') = \frac{\mu_{mgf} G'}{K_{mgf} + G'}$$

$$K_{go}(G') = \frac{\mu_{mgo} G'}{K_{mgo} + G'} \frac{O}{K_{mgd} + O},$$

$$K_{eo}(E') = \frac{\mu_{meo} E'}{K_{meo} + E'} \frac{O}{K_{med} + O} \frac{K_{inhib}}{K_{inhib} + G'}, \quad (13)$$

where O is the dissolved oxygen concentration; μ_{mgf}, μ_{mgo} and μ_{meo} are maximum consumption rates; K_{mgf}, K_{mgo}, K_{mgd}, K_{meo} and K_{med} are saturation constants; and K_{inhib} is a constant that characterizes the inhibitory effect of glucose on ethanol oxidation. The function $f(m)$ in Eq. (10) is used to model production of ethanol by budded cells:

$$f(m) = \begin{cases} 0 & m \leqslant m_t^* \\ \gamma_e \exp[-\varepsilon_e(m - m_t^* - m_e)^2] & m > m_t^* \end{cases} \quad (14)$$

where γ_e, ε_e and m_e are constant parameters.

The liquid phase oxygen balance is written as

$$\frac{dO}{dt} = K_{lo}a(O^* - O) \\ - \int_0^\infty \left[\frac{192}{180} \frac{K_{go}(G')}{Y_{go}} + \frac{96}{46} \frac{K_{eo}(E')}{Y_{eo}} \right] \\ \times W(m,t)\, dm, \quad (15)$$

where O^* is the saturation oxygen concentration, K_{lo} is the oxygen mass transfer coefficient, a is the interfacial area per unit liquid volume, the ratios $\frac{192}{180}$ and $\frac{96}{46}$ account for differences in molecular weights of the reactants and products. The oxygen solubility is assumed to be governed by Henry's law:

$$O^* = H_O RT O_{out}, \quad (16)$$

where H_O is the Henry's rate constant for oxygen, O_{out} is oxygen partial pressure in the gas exhaust stream, T is the absolute temperature, and R is the gas constant. The gas phase oxygen balance is

$$\frac{dV_g O_{out}}{dt} = F(O_{in} - O_{out}) - K_{lo}a(O^* - O)V_l, \quad (17)$$

where V_g and V_l are the gas phase and liquid phase volumes, respectively; F is the volumetric air feed flow rate; and O_{in} is the oxygen partial pressure in the air feed stream. The liquid phase carbon dioxide balance is

$$\frac{dC}{dt} = K_{lc}a(C^* - C) \\ + \int_0^\infty \left[\frac{264}{180} \frac{K_{go}(G')}{Y_{go}} + \frac{88}{46} \frac{K_{eo}(E')}{Y_{eo}} \right] \\ \times W(m,t)\, dm \\ + \int_0^\infty \left[f(m) \frac{88}{180} \frac{K_{gf}(G')}{Y_{gf}} \right] W(m,t)\, dm, \quad (18)$$

where C is the liquid phase carbon dioxide concentration, C^* is the saturation carbon dioxide concentration, K_{lc} is the carbon dioxide mass transfer coefficient, and the ratios $\frac{264}{180}$, $\frac{88}{46}$ and $\frac{88}{180}$ account for differences in molecular weights. The carbon dioxide solubility is modeled as

$$C^* = H_C(pH)RTC_{out}, \quad (19)$$

Table 1
Yeast cell population model parameters

Variable	Value	Variable	Value
H_O	0.0404 g/l/atm	H_C	1.48 g/l/atm
V_g	1 l	V_l	0.4 l
$K_l a$	1500 h^{-1}	$K_l c$	1500 h^{-1}
D	0.16 h^{-1}	G_f	20 g/l
E_f	0 g/l	F	10 l/h
T	298 K	O_{in}	0.21 atm
C_{in}	0.003 atm		
Y_{go}	0.15 g/g	μ_{mgo}	5×10^{-11} g/h
Y_{eo}	0.5 g/g	μ_{meo}	5×10^{-11} g/h
γ	400	ε	7
γ_e	8	ε_e	20
m_o	1×10^{-11} g	m_e	1×10^{-11} g
A	$\sqrt{10/\pi}$	β	40
S_l	0.1 g/l	S_h	2.0 g/l
K_t	0.01 g/g l	K_d	2 g/g l
m_{to}	6×10^{-11} g	m_{do}	11×10^{-11} g
K_{go}	0.002 g/l	K_{eo}	0.002 g/l
K_{mgf}	10 g/l	K_{mgo}	1 g/l
K_{meo}	0.1 g/l	K_{inhib}	1 g/l
K_{mgd}	0.002 g/l	K_{med}	0.002 g/l
α_g	20	α_e	20

where the carbon dioxide rate constant H_C is evaluated at a pH of 5.0, and C_{out} is the carbon dioxide partial pressure in the exhaust gas stream. The gas phase carbon dioxide balance is

$$\frac{\mathrm{d}V_g C_{out}}{\mathrm{d}t} = F(C_{in} - C_{out}) - K_{lc}a(C^* - C_{out})V_l, \qquad (20)$$

where C_{in} is the carbon dioxide partial pressure in the air feed stream. The model parameters listed in Table 1 are obtained from (Mhaskar et al., 2002).

3. Computational techniques

3.1. Numerical model solution

The cell population model presented in the previous section is comprised of a coupled set of nonlinear algebraic, ordinary differential and integro-partial differential equations. Numerical solution of the model is required to generate the spatiotemporal data required for construction of the reduced-order nonlinear models. The standard approach is to spatially discretize the PBE to obtain a finite number of nonlinear ordinary differential equations (ODEs) with time as the independent variable. A variety of numerical solution techniques based on finite difference, weighted residual and orthogonal collocation methods are available. An accurate approximation may require a large number of node points especially if there is more than a single dimension (Shvartsman & Kevrekidis, 1998). Zhu et al. (2000) use orthogonal collocation on finite elements to discretize a simplified version of the yeast cell population model presented in Section 2. The cell mass domain is discretized into a number of finite elements, each of which contains several collocation points where the PBE is approximated by an ODE. Integral terms are approximated using Gaussian quadrature. The state vector of the resulting nonlinear ODE model consists of the cell number density at each collocation point, as well as the substrate and effective substrate concentrations. To obtain a sufficiently accurate discretization, 12 finite element and 8 internal collocation points on each finite element are employed. In this paper, we apply this discretization scheme with the same number of discretization points to the cell population model presented in Section 2. The resulting model consists of 117 nonlinear ODEs.

3.2. Nonlinear model reduction

High-dimensional models such as a discretized cell population model are not amenable to dynamic analysis and model-based controller design. Fortunately, most high-dimensional models possess different time scales over which the dynamics evolve. The model is viewed as having "fast modes" and "slow modes" according to the location of the associated eigenvalues in the complex space (Khalil, 1996). As the transient effect of the fast modes has a short duration, the relevant dynamic behavior of the model is determined mainly by the slow modes. If a high-order model possesses only a few slow modes, then it is effectively a low-dimensional system. Using various model reduction techniques, the full-order model can be projected onto a much lower dimension subspace where the slow modes evolve. The resulting low-dimensional model should be a good approximation of the full-order model.

Because the discretized cell population model has a total of 117 nonlinear ODEs, it is too complex for effective analysis and control system design. However, 109 of the state variables represent the cell number distribution at different cell masses. As these state variables are highly correlated, it is envisaged that a significant dimensionality reduction is possible. As shown in Fig. 1, the cell population model has a large number of fast modes. These observations motivate an attempt to perform dimensionality reduction on the cell population model to facilitate future dynamic analysis and controller design studies.

Several nonlinear model reduction techniques have been proposed in the literature. They can be categorized into three groups: (i) methods based on approximate inertial manifolds (AIM) (Armaou & Christofides, 2000); (ii) methods based on POD (Holmes et al., 1997) and (iii) methods based on balanced truncation (Lall, Marsden, & Glavaski, 2002). The POD method is used in this paper since it has been shown to yield accurate reduced-order models while accounting for the effect of input changes on the system behavior (Shvartsman & Kevrekidis, 1998). The POD method was originally proposed by Lorenz (Lorenz, 1956) and has been popularized
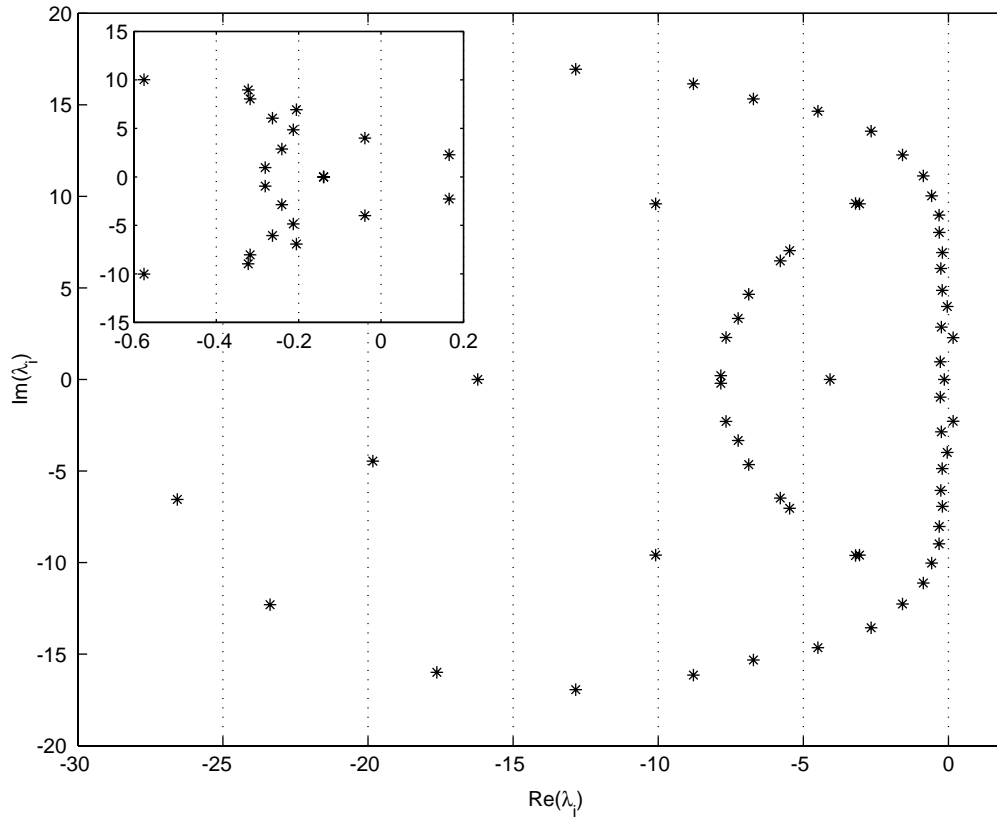
Fig. 1. Spectrum of the full-order model.

by Lumley and others (Holmes et al., 1997) for the study of dynamical features in complex fluid flows. More recently, POD has found wide application in solids and structures (Holmes et al., 1997), image processing (Sirovich, 1989) and the design of controllers for PDE systems (Shvartsman & Kevrekidis, 1998). Below we provide a brief outline of the POD method; a more detailed description can be found in (Holmes et al., 1997).

Consider a nonlinear system of the general form

$$\dot{x} = f[x(t), u(t)], \tag{21}$$

where $x \in \mathscr{R}^n$ and $u \in \mathscr{R}^m$ are the state and input vectors, respectively. The underlying idea of the POD method is to find an optimal low-dimensional linear subspace of the state space in which the relevant dynamics of the original system evolve. The method requires extensive spatiotemporal data, either from the actual process or from simulation of an accurate model. For a given sampled data set $\{x^{(1)}, \ldots, x^{(N)}\}$ of $x(t)$, define R as the correlation matrix of the data

$$R := \sum_{i=1}^{N} x^{(i)} x^{(i)*}, \tag{22}$$

where $x^{(i)}$ is the ith snapshot of the state variables in the data set and $x^{(i)*}$ is the complex conjugate of $x^{(i)}$. Let $\lambda_1 \geqslant \lambda_2 \geqslant \cdots \lambda_n$ be the eigenvalues of R, k be the rank of R, and $\phi_1, \phi_2, \ldots, \phi_k$ be orthogonal eigenvectors of R

corresponding to the nonzero λ_i. Each vector $x^{(i)}$ can be written as

$$x^{(i)} = \sum_{j=1}^{k} \alpha_{ij} \phi_j,$$

where $\alpha_{ij} = \langle x^{(i)}, \phi_j \rangle$, and $\langle \phi_i, \phi_j \rangle = \delta_{ij}$. The optimal s-dimensional subspace approximation of the original state variables is given by

$$\hat{x}^{(i)} = \sum_{j=1}^{s} \alpha_{ij} \phi_j. \tag{23}$$

Denote $P := [\phi_1, \phi_2, \ldots, \phi_s]^{\mathrm{T}}$ as the transformation matrix. The projection of x on the subspace $S = \mathrm{span}\{\phi_1, \phi_2, \ldots, \phi_s\}$ can be written as $y = Px$ where y is a representation of x in the new coordinates ϕ_i. The approximation of x is given by $\hat{x} = P^*Px \in S$ where P^* is the complex conjugate of P. This subspace approximation is optimal in the sense that the "total energy" preserved

$$p = \frac{\sum_{i=1}^{s} \lambda_i}{\sum_{i=1}^{n} \lambda_i} \tag{24}$$

is maximized. The number of principal components s retained in the reduced-order model should be chosen such that $p \cong 1$ to ensure good approximation of the full-order system.

Galerkin projection has been used extensively to construct reduced-order mathematical models of dynamical systems (Holmes et al., 1997). The basic idea is to project the full-order vector field on the tangent space of a s-dimensional subspace $S \subset \mathcal{R}^n$ of the original state space. Using the coordinates obtained from the POD methods, the resulting reduced-order approximation is given by

$$\dot{y}(t) = Pf[P^* y(t), u(t)]. \tag{25}$$

The POD-Galerkin method projects the dynamics onto the subspace containing most of the "energy" of the system. If all the eigenvectors corresponding to the nonzero eigenvalues of the correlation matrix R are retained, then this subspace will contain all the local dynamics. Clearly there is a trade-off between the extent of model reduction and the quality of the reduced-order model. The goal is to utilize as few basis functions as possible to ensure an "acceptable" approximation of the full-order dynamics.

In summary, the POD-Galerkin model reduction method involves:

1. Collection of a representative set of spatiotemporal process or model simulation data.
2. Extraction of an empirical eigenfunction basis from the data.
3. Construction of a reduced-order dynamical system by projection of the full-order vector field onto these basis functions.

The empirical nature of the method suggests that the first step is crucial for generating a useful approximate model. The data ensemble is the starting point for forming the reduced-dimensional subspace onto which the original state space is projected by the Galerkin procedure. All dynamics orthogonal to this subspace are neglected under the assumption that the resulting error will be "small". In addition to the necessity for a large spatiotemporal data set, there are no a priori comprehensive guidelines for generation of a suitable ensemble from which the empirical basis functions will be extracted. A potentially representative ensemble can be obtained by combining spatiotemporal motions at several values of key operating parameters, mixing transients from different initial conditions distributed randomly around relevant regions of the phase space and collecting responses to perturbation of actuators from their nominal settings. Additional guidelines for spatiotemporal data collection are discussed elsewhere (Aling, Ebert, Naeini, & Kosut, 1996; Deane, Kevrekidis, Karniadakis, & Orszag, 1991; Graham & Kevrekidis, 1991; Park & Cho, 1996; Shvartsman & Kevrekidis, 1998).

Because we are primarily interested in capturing oscillatory dynamics of the cell population model, it is necessary to include transient data as well as stationary data. Our ultimate goal is to develop a reduced-order model (ROM) suitable for model-based controller design. The ROM is required to provide reasonable predictions over a large oper-

ating regime. Consequently, it is necessary to incorporate simulation data for several parameter values that span the desired region of operation.

3.3. Bifurcation analysis

In our previous publications (Zhang & Henson, 2001; Zhang et al., 2002) we have argued that bifurcation analysis allows more efficient and insightful analysis of bioreactor model behavior than is possible with dynamic simulation alone. The same argument applies to comparison of full-order model (FOM) and reduced-order model behavior. If a ROM has a bifurcation structure that closely matches that of the FOM, then the ROM is a good candidate for further analysis. It is important to note that bifurcation analysis only allows investigation of the long-term model dynamics. Therefore, dynamic simulation is necessary to analyze the short-term dynamic behavior.

In this paper, only steady state and periodic solutions of the yeast cell population model are studied. Steady-state solutions are located using the nonlinear equation solver NNES. Eigenvalues of the Jacobian matrix are computed at each steady state to determine the local stability. A steady state where one or more eigenvalues cross the imaginary axis is known as a bifurcation point (Kuznetsov, 1995). A continuation code based on the shooting method is used to locate periodic solutions and to determine their stability. The code requires a good initial guess of the state variables and the oscillation period at a particular operating condition. Such an initial point is readily obtained for a stable periodic solution by dynamic simulation. The ODE solver ODESSA is used for numerical integration. Limit cycles at different operating conditions can then be found via continuation. Stability of the periodic solutions is determined by examining the Floquet multipliers of the Poincaré map.

4. Results and discussion

4.1. Full-order model

In our previous work (Mhaskar et al., 2002), we have demonstrated via dynamic simulation that the yeast cell population model can predict the coexistence of stable steady state and stable periodic solutions at the same operating conditions as has been observed experimentally (Zamamiri, Birol, & Hjortso, 2001). Figs. 2 and 3 illustrate dynamic responses of the model for the inputs $D = 0.14 \text{ h}^{-1}$ and $S_f = 30 \text{ g/l}$ starting from two different initial conditions. An initial distribution that leads to a stable steady-state solution is shown in the top plot of Fig. 2. As shown in the bottom plot, the initial distribution is sufficiently dispersed for the oscillations to slowly decay. Note that the final distribution shown in the top plot is very dispersed as compared to the initial distribution. A slightly less dispersed initial distribution that leads to sustained oscillations is shown in the top
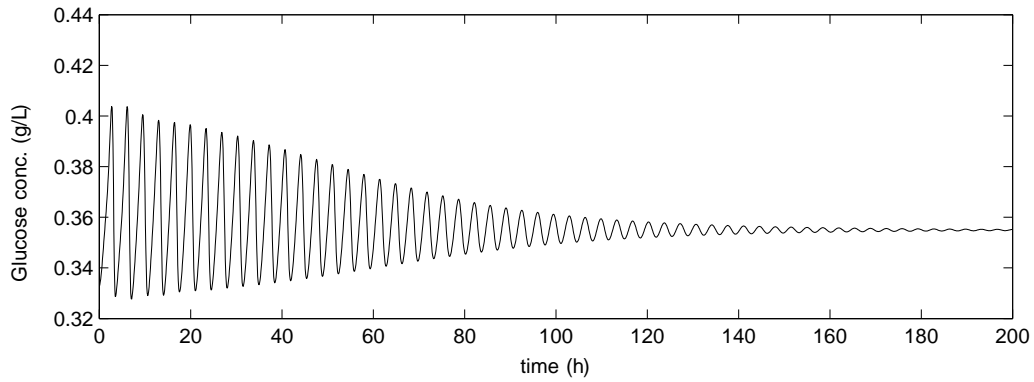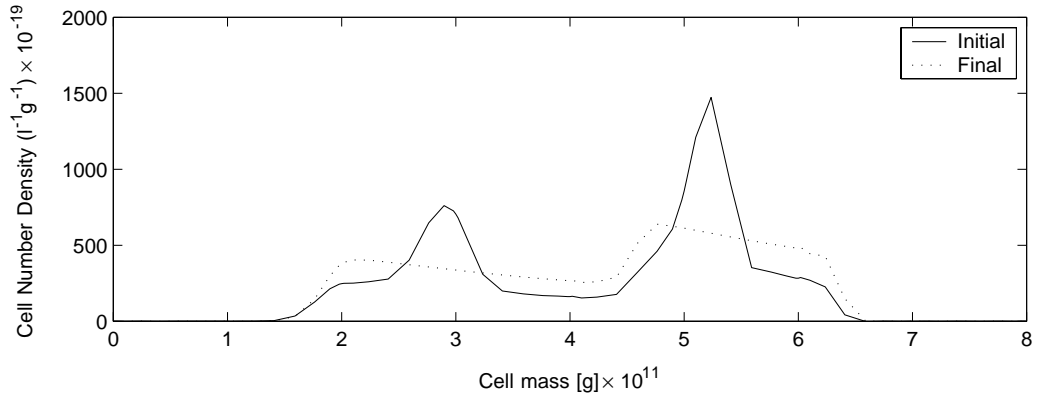
Fig. 2. Transient response of the full-order model decaying to a steady-state solution.
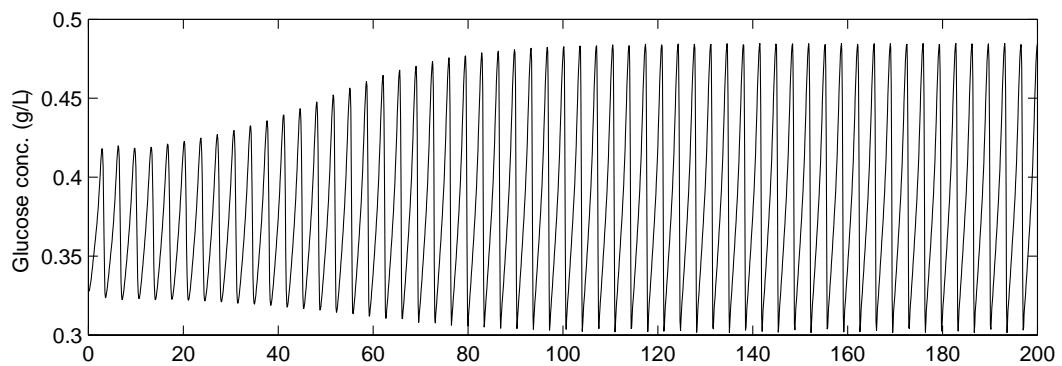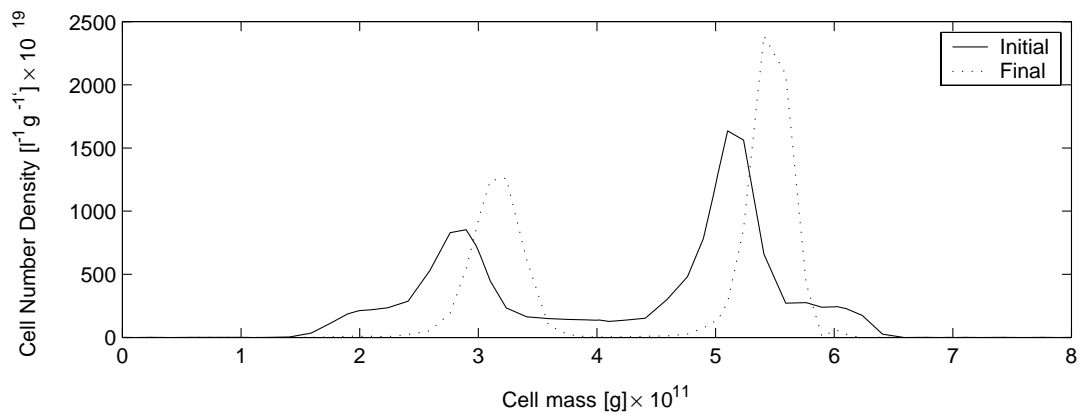

Fig. 3. Transient response of the full-order model growing to a sustained oscillation.
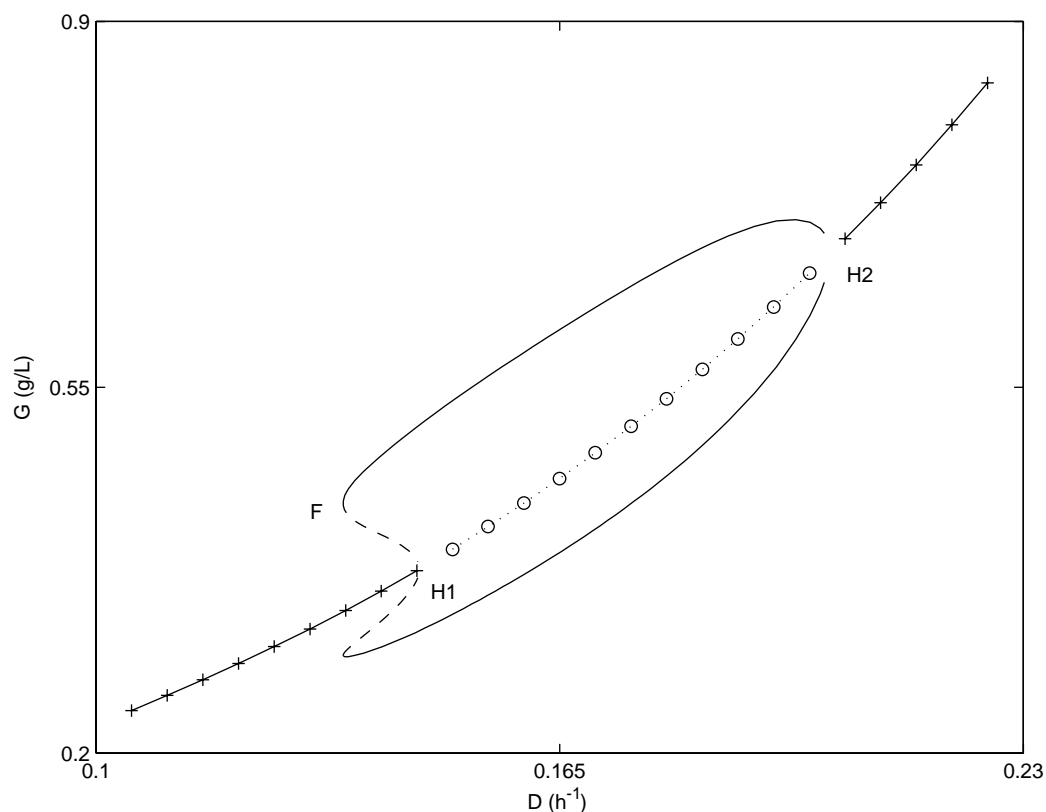
Fig. 4. Bifurcation diagram of the full-order model.

plot of Fig. 3. In this case, the oscillation amplitude grows until a stable periodic solution is obtained. Two well defined peaks that correspond to daughter and mother cell subpopulations are present in the final distribution. These tests confirm that the model is consistent with experimental observations that sustained oscillations are intimately related to cell cycle synchrony (Strassle, Sonnleitner, & Fiechter, 1988) and the formation of distinct cell subpopulations. Both attractors have significant regions of attraction, as will be verified by the bifurcation analysis results presented below. Given their similarity, the initial distributions shown in Figs. 2 and 3 appear to be near the separatrix that divides the domains of attraction of the two solutions.

A bifurcation diagram for the full-order model is shown in Fig. 4 where the dilution rate (D) is the bifurcation parameter and the glucose concentration (G) is chosen as a representative output variable. The model possesses a single stable steady-state solution ($+$) at low dilution rates. As the dilution rate is increased, a bifurcation (H1) occurs where the steady-state solution becomes unstable ($\circ$) and a stable periodic solution with oscillations of the amplitude indicated ($-$) appears. This Hopf bifurcation is accompanied by the appearance of large amplitude oscillations. The stable periodic solution and the unstable steady-state solution coexist over a large range of dilution rates. As the dilution rate is increased further, a second bifurcation (H2) occurs

where the periodic solution disappears and the steady-state solution regains its stability. This Hopf bifurcation is characterized by small amplitude oscillations. The Poincaré map indicates that the upper bifurcation is supercritical since all multipliers lie inside the unit circle, while the lower Hopf bifurcation is subcritical due to the presence of one Floquet multiplier outside the unit circle. It also discloses that the periodic solution branch undergoes a fold bifurcation (F) and changes its stability when one Floquet multiplier crosses the unit circle. Note that there is a small range of dilution rates $D \in (0.135,\ 0.145\ \text{h}^{-1})$ near the subcritical bifurcation that supports both stable steady state and periodic solutions. The domains of attraction of the two solutions are separated by an unstable periodic solution with oscillations of the amplitude indicated ($- - -$) and its unstable manifold. This diagram provides a simple explanation for the dynamic simulation results presented above as the operating conditions are located in this range. It is important to note that our previously published model without the structured medium description (Zhu et al., 2000) does not exhibit a subcritical Hopf bifurcation. Therefore, the current model represents a significant improvement because it more faithfully reproduces experimentally observed behavior.

Before performing POD-Galerkin model reduction, it is useful to investigate the spectrum of the FOM to determine if such a reduction is expected to be beneficial; i.e.,
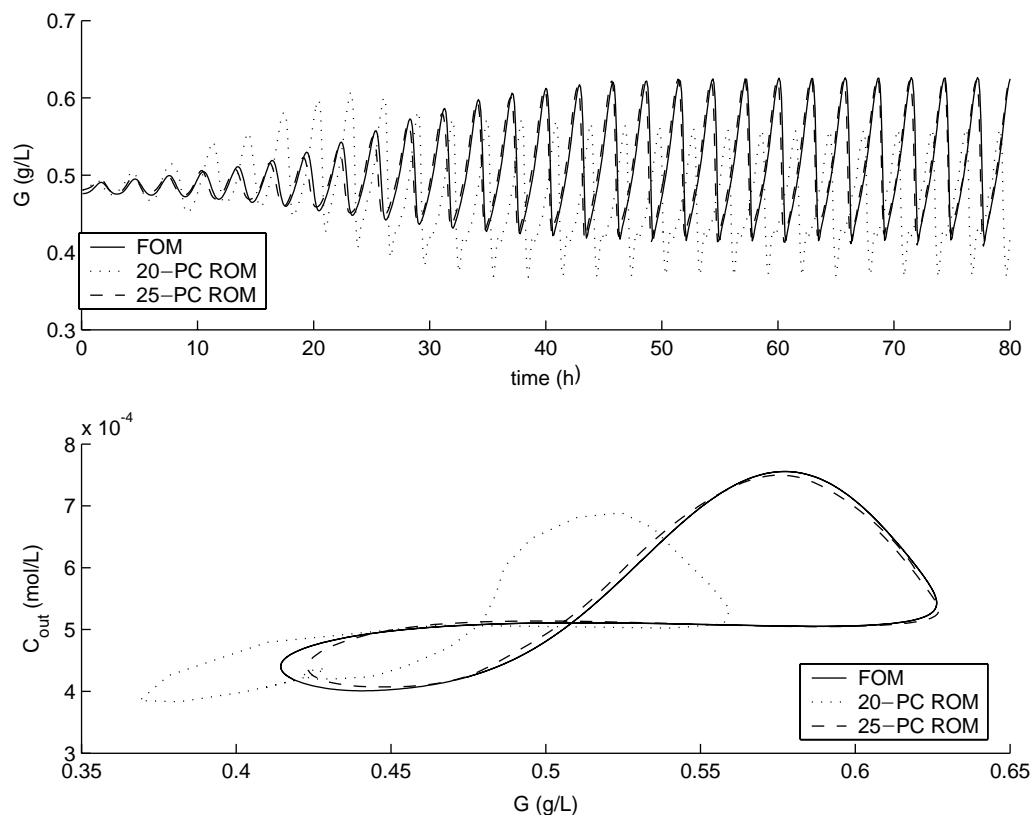
Fig. 5. Performance of ROMs based on a single data set at $D = 0.17 \text{ h}^{-1}$.

if the discretized model has a large number of fast modes and a small number of slow modes. Fig. 1 shows the spectrum of the FOM at an unstable steady-state solution where $D = 0.15 \text{ h}^{-1}$ and $S_f = 30 \text{ g/l}$. The model has a total of 117 eigenvalues, many of which have very large negative real parts. For clarity, only the 64 eigenvalues which have real parts greater than -30 are shown in the figure. As shown in the inset, there are also approximately 20 slow modes corresponding to eigenvalues which have real parts greater than -0.5. Investigation of the model spectrum at different operating conditions yields similar results. This suggests that the ROMs derived will require on the order of 20 basis functions to produce accurate predictions. Also note that the arrangement of eigenvalues suggests the possible existence of continuous and discrete spectrum for this problem. The Hopf bifurcation is clearly associated with discrete spectrum crossing and results in coherent oscillations of the population. The observation of possibly continuous spectrum relatively close to the imaginary axis is worth further exploration since it may have implications for the separation of time scales in the system.

4.2. Reduced-order model: single data set

Before presenting the ROM results, a few practical issues involved in applying the POD-Galerkin method are

discussed. First, we have found that it is important to scale the FOM state variables such that they have comparable magnitude. Since the POD method is concerned only with the "total energy" in the data ensemble, important variables with small magnitude may not be adequately reflected in the ROM in the absence of scaling. In fact, we failed to generate useful ROMs with unscaled raw data. Second, we have used the scaled raw data directly for ROM construction. Some researchers (Deane et al., 1991; Lall et al., 2002). have suggested that the ensemble mean should be subtracted from the data before model reduction. For a single data set, we have found that this approach provides no discernible advantage. Furthermore, the ensemble mean does not have a physical meaning when multiple data sets at different parameter values are combined to generate a "global" reduced-order model. Therefore, we have not subtracted the mean value from the data ensemble.

To study the effectiveness of POD-Galerkin model reduction, a ROM derived from a single set of transient simulation data at a fixed operating condition ($D = 0.17 \text{ h}^{-1}$ and $S_f = 30 \text{ g/l}$) is first studied. The training data set consists of 600 snapshots of the 117 state variables during the first 60 h of the open-loop simulation shown in the first subplot of Fig. 5. This data set contains information on both the transient phase and the fully developed oscillations. A ROM constructed from this data set is expected to capture
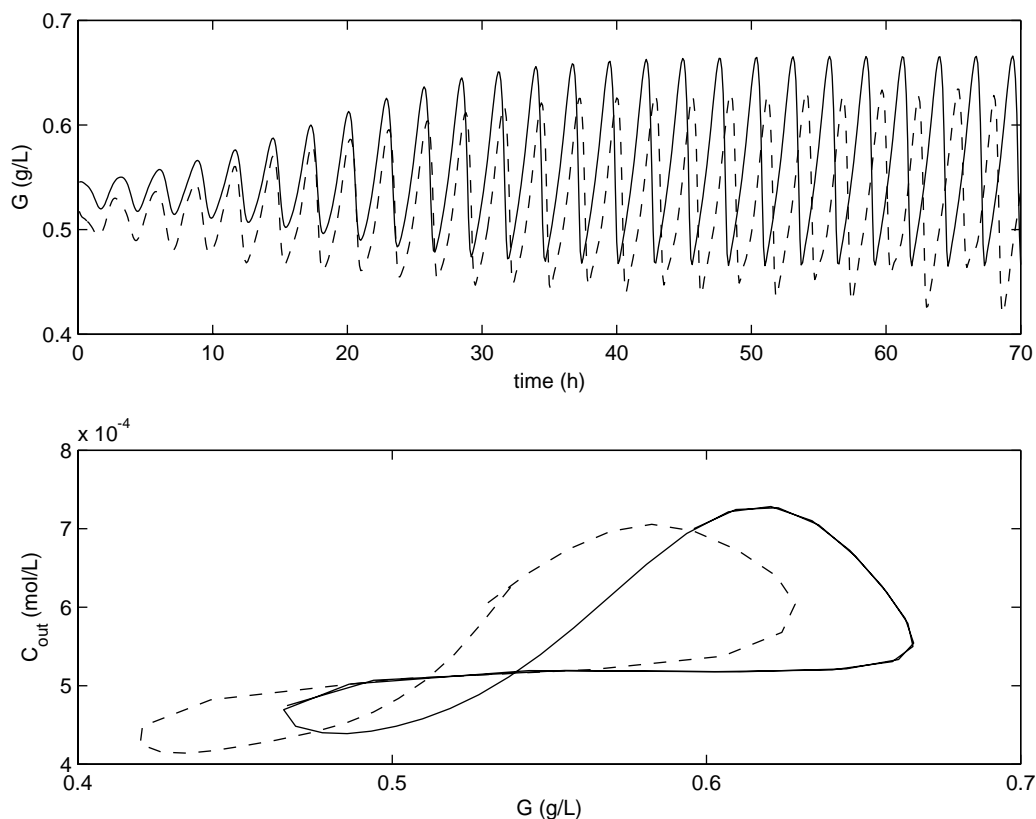
Fig. 6. Transient response of the 25-PC ROM for $D = 0.18$ h^{-1}.

both the short-term and long-term dynamics of the FOM. A variety of ROMs with different numbers of principal components (PCs) were constructed and compared to the FOM. The results are summarized below:

- $\leqslant 6$ PCs: integrator fails to converge.
- 7–8 PCs: the transient response exhibits large errors, while the sustained oscillations have an amplitude comparable to that of the full-order model. The mean value of the fully developed oscillations has significant offset.
- 9–16 PCs: integrator fails to converge.
- 18–20 PCs: the ROMs yields reasonably accurate predictions.
- 25+ PCs: the ROMs yields almost perfect predictions.

The need to maintain approximately 20 PCs to obtain an accurate ROM is not particularly desirable, but it is consistent with the earlier analysis of the model spectrum. The result that ROMs with 7 or 8 PCs can yield reasonable results while ROMs with 9–16 PCs fail is surprising. Although not studied here, additional order reduction may be possible with more advanced techniques such as nonlinear Galerkin projection (Aling et al., 1997).

Fig. 5 provides a comparison of two ROMs with 20 and 25 PCs with the FOM. The original 117 state variables are reconstructed from the ROM simulation results, and the re-

constructed glucose concentration is plotted in the figure. The 25-PC ROM provides a very good match to the FOM, both in terms of short-term transients and long-term sustained oscillations. The 20-PC ROM not only inaccurately predicts the short-term dynamics, but it also yields sustained oscillations with an incorrect period and a significant offset in mean glucose concentration as compared to the FOM. Phase portraits corresponding to sustained oscillations of the three models are shown in the lower subplot of Fig. 5 where the glucose concentration (G) and the gas phase CO_2 concentration (C_{out}) are selected as representative variables. The 20-PC ROM exhibits large errors, while the trajectory for the 25-PC ROM is almost identical to that of the FOM. Extensive simulation tests confirm that ROMs based on 25+ PCs also provide very accurate predictions.

A validation test is performed to evaluate the ability of the 25-PC ROM to predict dynamic behavior under different operating conditions. Fig. 6 shows an open-loop simulation for $D = 0.18$ h^{-1} and $S_f = 30$ g/l. The ROM does not effectively capture the dynamic behavior of the FOM at this operating condition. Because the ROM ultimately will be used for model-based controller design, it is clear that a single data set at a fixed dilution rate will not be satisfactory. Additional FOM data representing the operating regime of interest must be collected for the ROM to yield accurate predictions over a meaningful range of dilution rates.
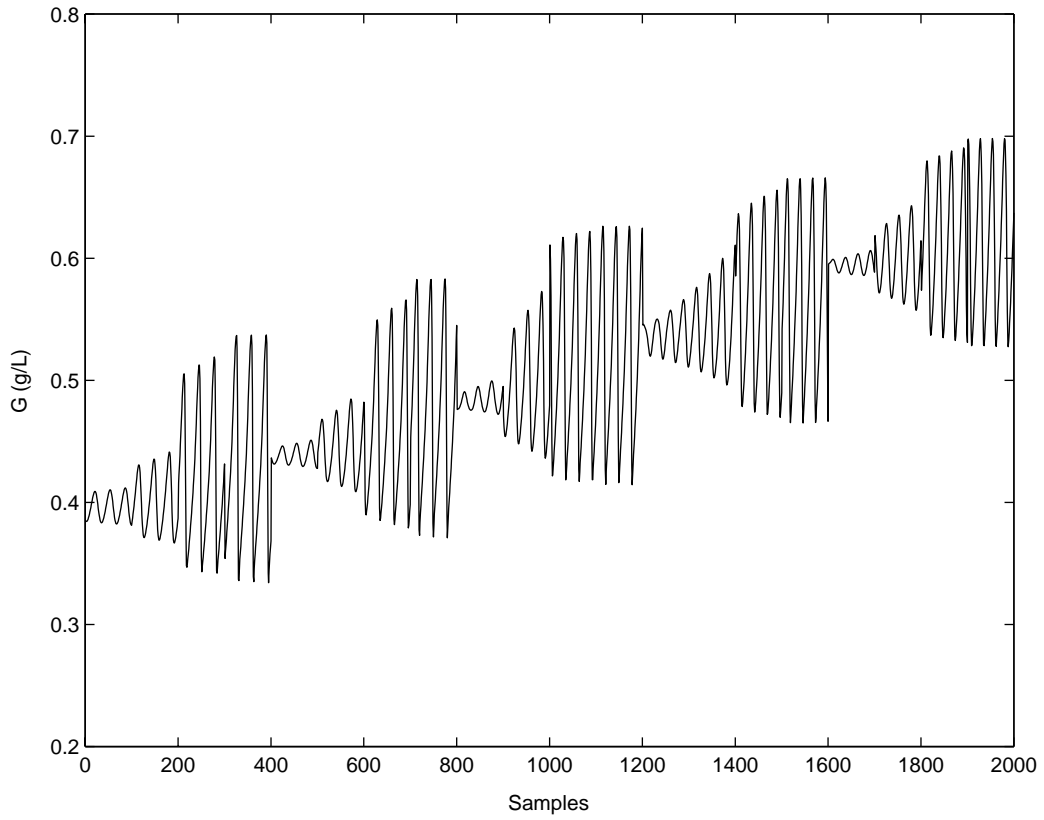
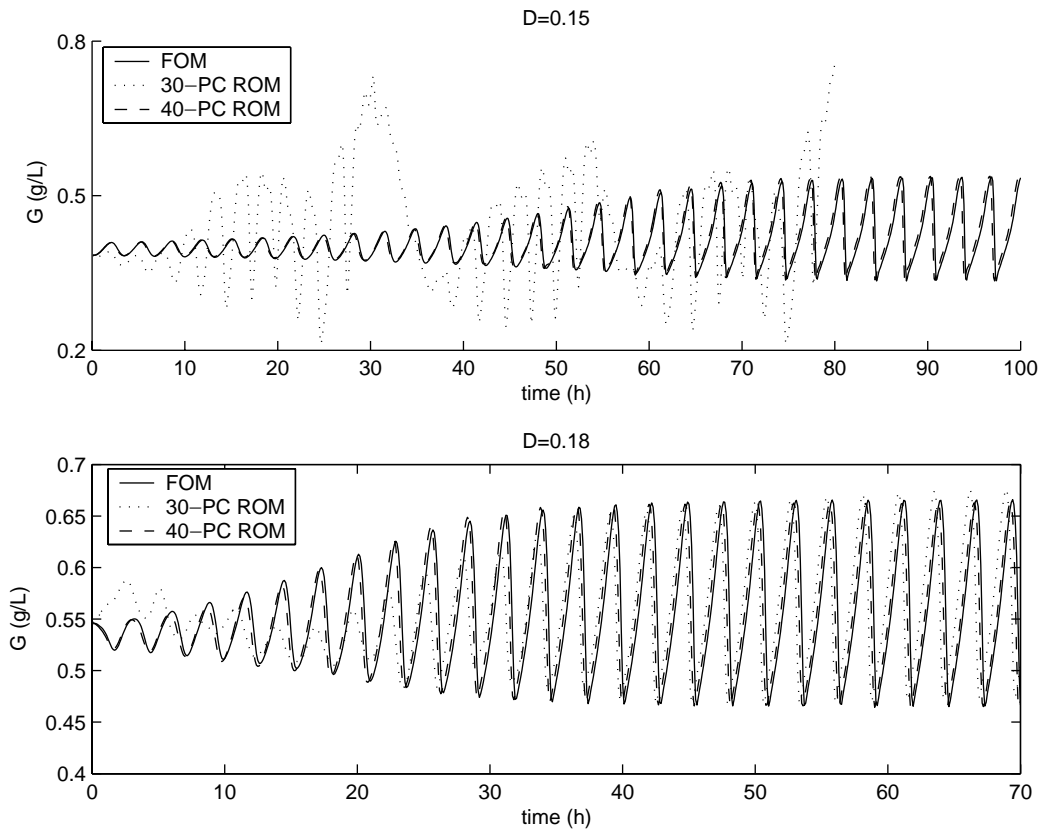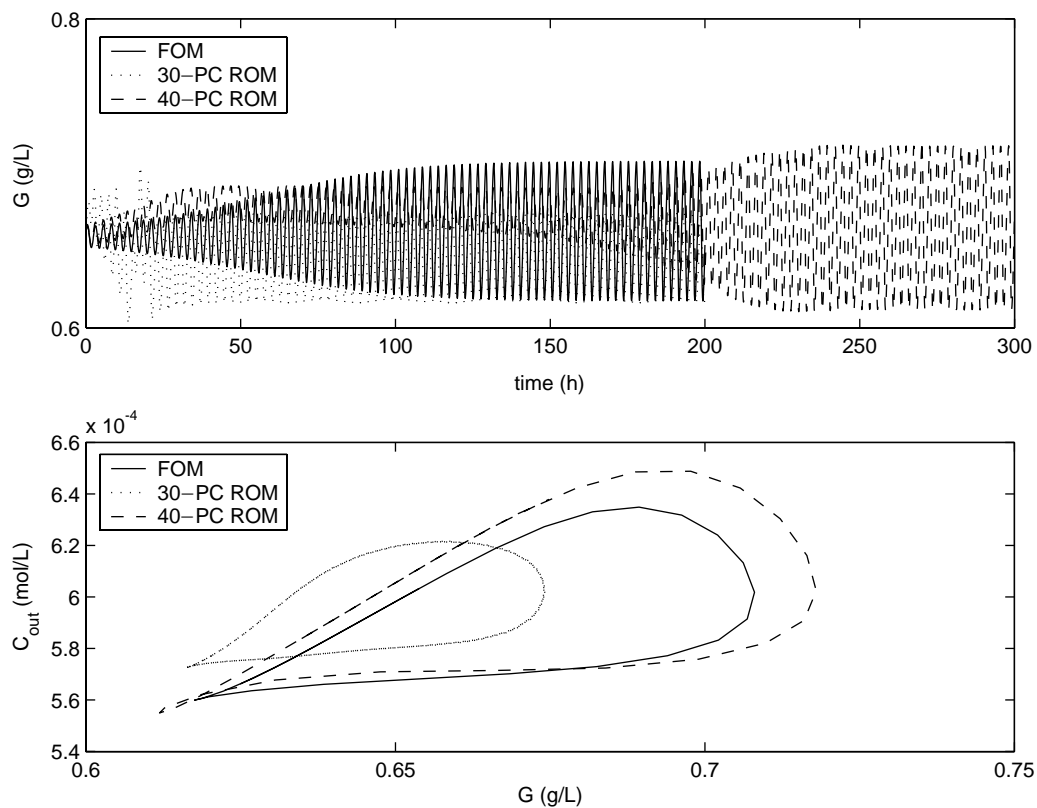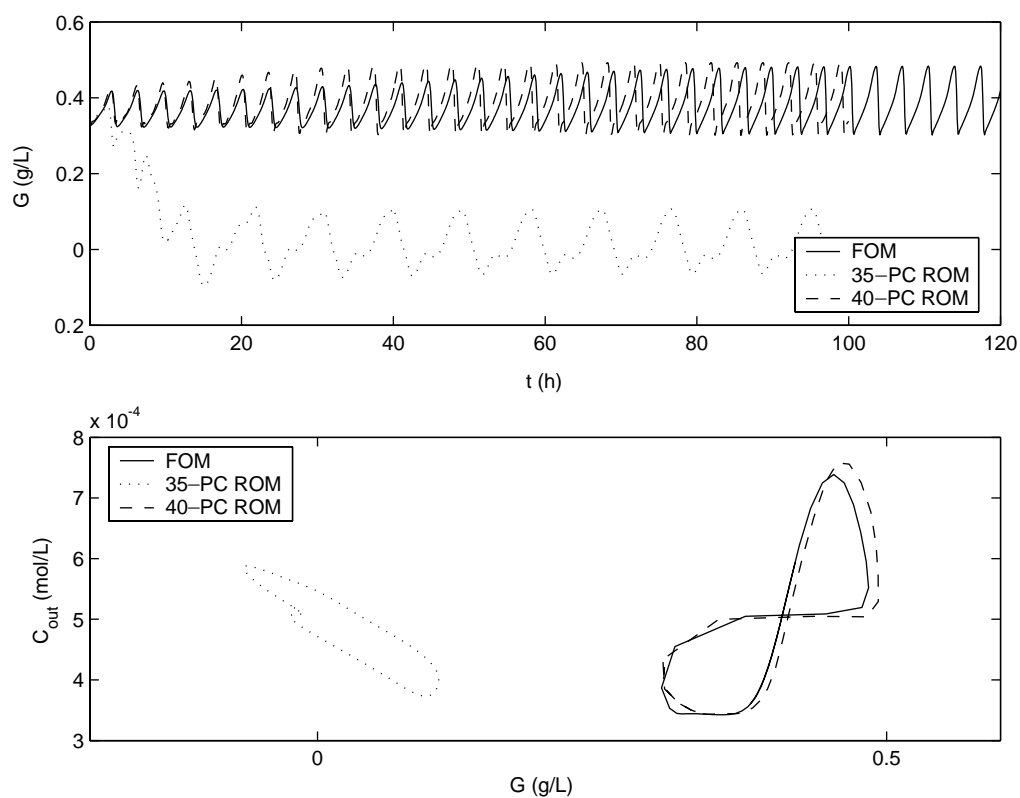Fig. 7. Training data set for oscillatory ROM construction.

Fig. 8. Performance of ROMs within the training range.

Fig. 9. Performance of ROMs outside the training range for $D = 0.20$ h^{-1}.

Fig. 10. Performance of ROMs outside the training range for $D = 0.14$ h^{-1}.

4.3. Reduced-order model: oscillatory range

Fig. 7 shows a training data set consisting of five sets of transient data obtained from open-loop simulations of the FOM under different operating conditions that support sustained oscillations. The data sets are generated by fixing S_f at 30 g/l and setting D at five different values: 0.15, 0.16. 0.17, 0.18, and 0.19 h^{-1}. Each data set consists of 400 snapshots of the FOM state variables at different phases of the simulation where the oscillations have very small amplitude (100 points), the oscillations are somewhat developed (100 points), the oscillations are almost fully developed (100 points) and the oscillations are fully developed (100 points). Data sets are constructed in this manner to avoid large data sets that would result from direct sampling of an oscillatory simulation. By including transient responses and sustained oscillations at different operating conditions, the derived ROMs are expected to capture the short-term and long-term dynamics more "globally" than is possible with a single data set.

Fig. 8 provides a comparison of two ROMs derived from the data set in Fig. 7 and the FOM for two dilution rates ($D = 0.15$, 0.18 h^{-1}) contained within the training data set. The 40-PC ROM produces an almost perfect match of the glucose concentration dynamics. The 30-PC ROM provides satisfactory approximation for $D = 0.18$ h^{-1}, but it is unstable for $D = 0.15$ h^{-1}. Extensive simulation studies verify that ROMs with 40+ PCs also yield highly accurate approximation. Figs. 9 and 10 compare the ROM and FOM responses for two operating conditions outside the range of the training data set ($D = 0.20$, 0.14 h^{-1}). The 40-PC ROM provides reasonably accurate extrapolation, while the 30-PC or 35-PC ROM is not able to accurately reproduce the FOM dynamics.

Bifurcation analysis allows a more detailed study of the long-term dynamics of the ROMs. Fig. 11 shows a comparison of the one-parameter bifurcation diagrams of the 35-PC and 40-PC ROMs and the FOM. Within the oscillatory range, the unstable steady-state solutions of the 40-PC ROM are quite close to those of the FOM. The predicted steady states outside the oscillatory region are less accurate due to a lack of training data. The amplitudes of the 40-PC ROM limit cycles match those of FOM quite accurately over a large range of dilution rates. Furthermore, the 40-PC ROM correctly predicts the existence of the two Hopf bifurcations with the lower bifurcation being subcritical and the upper bifurcation being supercritical. The locations of the two bifurcation points are very close to those of the FOM. On the other hand, the 40-PC ROM predicts a significantly larger operating space where stable steady state and stable periodic solutions coexist. These results demonstrate that the 40-PC ROM represents a good approximation of the FOM despite lack of training data outside the oscillatory region. To achieve better agreement at lower dilution rates within the oscillatory region and for dilution rates outside the oscillatory region, it is necessary to utilize a more complete training data set. The predictions of the 35-PC ROM are far less satisfactory. In particular, the 35-PC ROM does not capture the lower Hopf bifurcation or the existence of multiple stable solutions. Consequently, this model is useful only in the upper range of oscillatory solutions.

4.4. Reduced-order model: global behavior

Fig. 12 shows a training data set used to obtain better predictions of the global FOM behavior. A total of six distinct data sets, each with 400 snapshots, are utilized. The data sets are collected at the same feed substrate concentration $S_f = 30$ g/l and six different dilution rates D of 0.13, 0.14, 0.16, 0.18, 0.20 and 0.21 h^{-1} from left to right in the figure. For dilution rates $D = 0.13$ h^{-1} and 0.21 h^{-1} where the FOM has only one stable steady-state solution, each data set consists of 300 snapshots of oscillations decaying to the steady state and 100 snapshots of the steady-state solution itself. For $D = 0.14$ h^{-1} where multiple stable solutions are supported, the data ensemble contains 200 snapshots of growing oscillations and sustained oscillations and 200 snapshots of decaying oscillations and the steady-state solution. For the other three dilution rates where only sustained oscillations exist, the data ensemble is constructed as in Fig. 7.

Fig. 13 provides a comparison of the transient responses of 35-PC and 40-PC ROMs and the FOM at $D = 0.18$ h^{-1}. With 40 basis functions retained, the ROM predictions are very close to those of the FOM. By contrast, the ROM with 35 PCs is not able to approximate the plant dynamics. Fig. 14 shows a comparison of the 40-PC ROM and the FOM at $D = 0.14$ h^{-1} for the set of initial conditions shown in Figs. 2 and 3. The FOM initial conditions are mapped into the reduced-dimensional space using the transformation matrix P to generate the initial conditions for the ROM. The ROM captures the convergence to the two different solutions, although the transient responses exhibit some small errors. Although not shown in the figure, it is worth mentioning that open-loop simulations with the 35-PC ROM lead to integration failure.

Fig. 15 shows the bifurcation diagrams for 40-PC and 50-PC ROMs and the FOM. The 40-PC ROM provides very close agreement near the lower bifurcation point, including the predicted range of multiple stable solutions and the predicted steady-state solutions outside the oscillatory range. This is attributable to utilizing a more global data set for ROM construction. This improved predictive capability is accompanied by less accurate predictions near the upper bifurcation point. In comparison, the 50-PC ROM is slightly better in predicting the oscillation bounds but less accurate in locating the lower Hopf bifurcation point and the fold bifurcation point of the periodic solutions. Many other tests of ROMs with different principal components have been performed. The ROMs with higher number of basis functions showed little improvement in approximating the overall
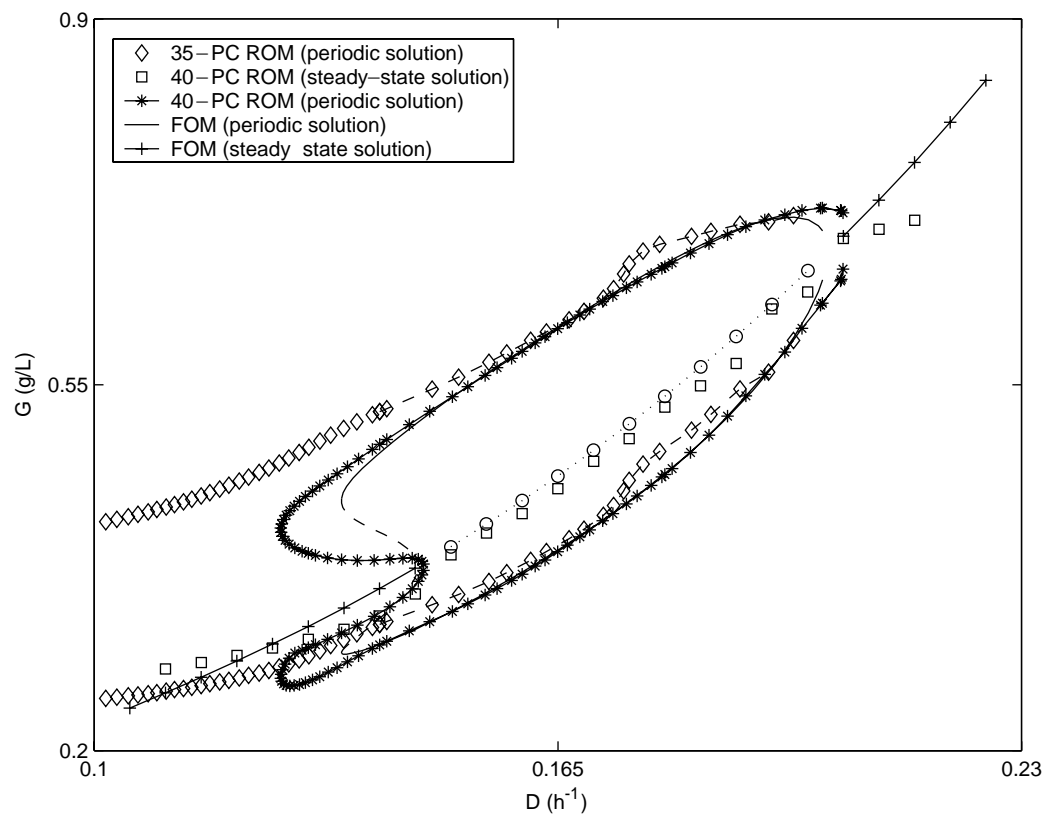
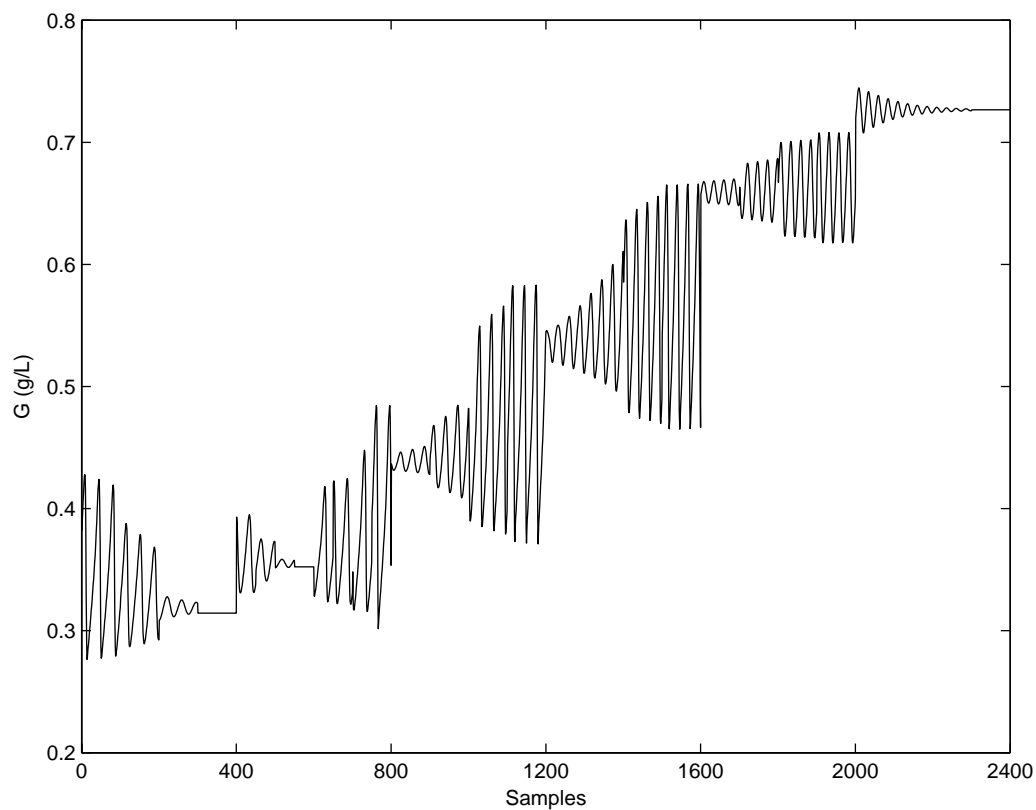Fig. 11. Bifurcation diagram of ROMs constructed from multiple data sets within the oscillatory range.

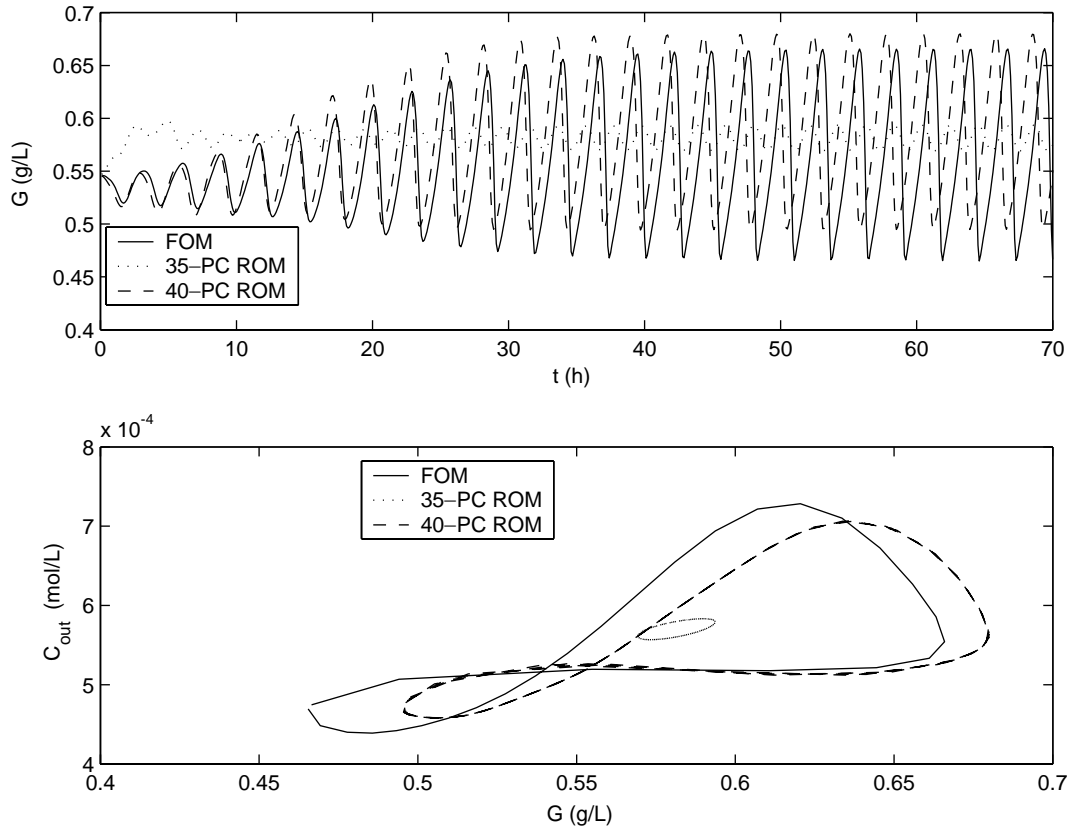Fig. 12. Training data set for global ROM construction.

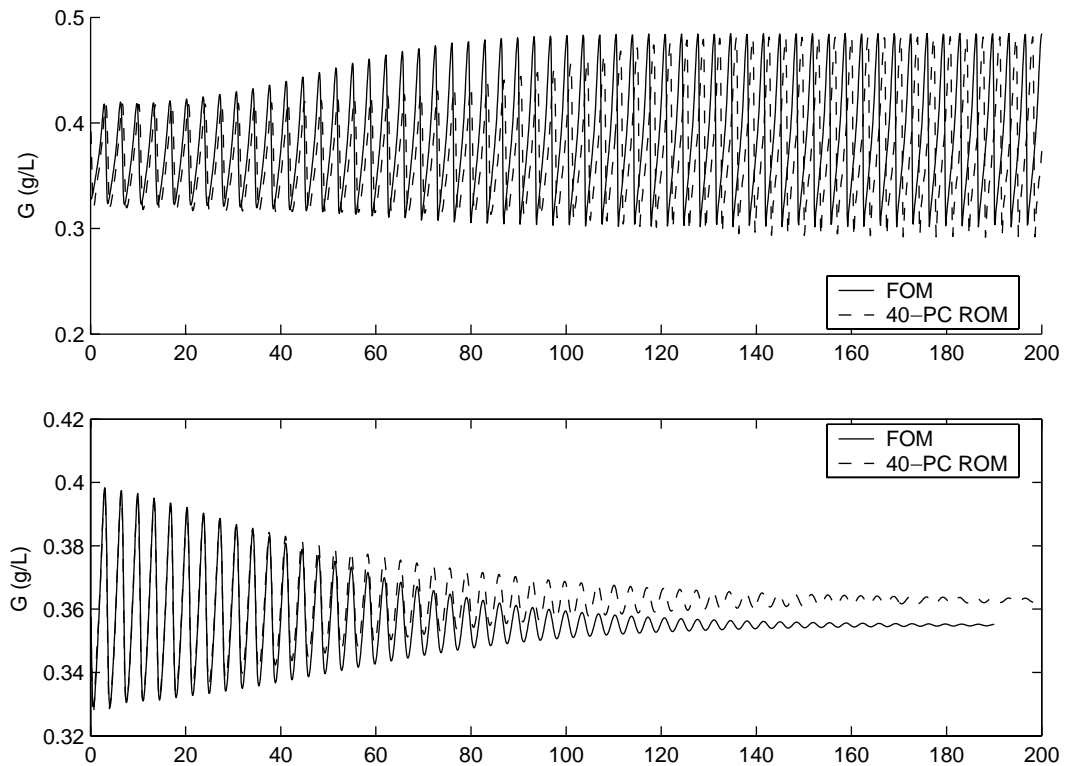Fig. 13. Performance of the global ROMs for $D = 0.18 \ h^{-1}$.

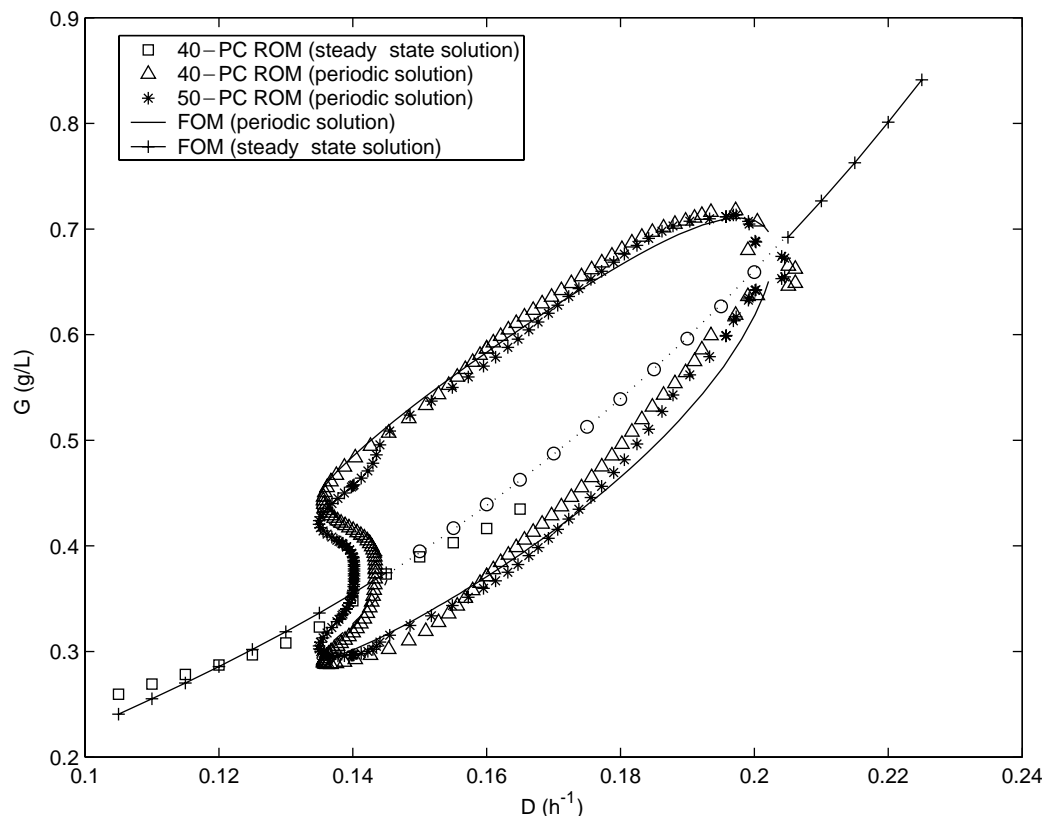Fig. 14. Performance of the global ROMs for $D = 0.14 \ h^{-1}$.

Fig. 15. Bifurcation diagram of ROMs constructed from global data set.

bifurcation diagram over the 40-PC ROM. Taking the computational cost into consideration, we believe that the 40-PC ROM represents a good approximation of the FOM.

Now we provide a few comments on the differences between the 40-PC ROM built from the oscillatory data set (Fig. 11) and the 40-PC ROM built from the global data set (Fig. 15). The former model provides more accurate prediction of the upper and lower oscillation limits over a wide operating range, while the latter model is superior in capturing the locations of the two bifurcation points. These results are attributable to differences between the training data sets since the approximation capability is highly dependent on the data used. As the relative weighting of oscillatory data in the global data set is significantly reduced with the introduction of data outside the oscillatory range, the prediction accuracy of the oscillation amplitudes is expected to be sacrificed. Clearly, a different data set could be constructed to obtain a ROM which provides better predictions in the oscillatory range at the expense of less accurate predictions of the bifurcations point locations.

These results again emphasize that the POD method is empirical and data-driven. The training data sets used in this study are admittedly heuristic, albeit they are chosen according to some reasonable guidelines. Therefore, the ROM obtained cannot be considered as optimal in a practical sense. Furthermore, the choice of satisfactory ROMs is based largely on individual judgment. General guidelines include,

but are not limited to short-term versus long-term prediction capabilities, dimension versus model accuracy and model accuracy versus model robustness.

5. Summary and conclusions

We have studied model order reduction of a discretized yeast cell population balance model using a combination of proper orthogonal decomposition (POD) and Galerkin projection. The collection of a representative spatiotemporal data set from which the basis functions of the reduced-order model (ROM) are constructed was shown to be critical. Dynamic simulation and bifurcation analysis results demonstrate that accurate ROMs can be generated with roughly one-third of the differential equations of the full-order model. The ROMs yield very good short-term and long-term predictions over a wide range of operating conditions. Despite the significant dimensionality reduction, accurate ROMs are composed of approximately 40 nonlinear differential equations. Consequently, additional order reduction methods such as nonlinear Galerkin projection (Aling et al., 1997) are currently being pursued. In particular, we plan to explore the interplay of low-dimensionality and the continuous spectrum suggested in Fig. 1. Additional future work will focus on the use of ROMs for model-based control of continuous yeast bioreactors.

Acknowledgements

References

Aling, H., Banerjee, S., Bangia, A. K., Cole, V., Ebert, J. L., Emami-Naeini, A., Jensen, K. F., Kevrekidis, I. G., & Shvartsman, S. (1997). Nonlinear model reduction for simulation and control of rapid thermal processing. In *Proceedings of the American Control Conference*, Albuquerque, NM (pp. 2233–2238).

Aling, H., Ebert, J. L., Naeini, A. E., & Kosut, R. L. (1996). Application of nonlinear model reduction to rapid thermal processing reactor. In *Proceedings of the International Rapid Thermal Processing Conference*, Amsterdam, Netherland (pp. 356–361).

Armaou, A., & Christofides, P. D. (2000). Wave suppression by nonlinear finite-dimensional control. *Chemical Engineering Science*, *55*, 2627–2640.

Deane, A. E., Kevrekidis, I. G., Karniadakis, G. E., & Orszag, S. A. (1991). Low-dimensional models for complex geometry flows: Application to grooved channels and circular cylinders. *Physics of Fluids*, *3*, 2337–2354.

Eakman, J. M., Fredrickson, A. G., & Tsuchiya, H. M. (1966). Statistics and dynamics of microbial cell populations. *Chemical Engineering Progress Symposium Series*, *62*, 37–49.

Foias, C., Sell, E. S., & Temam, R. (1988). Inertial manifolds for nonlinear evolutionary equations. *Journal of Differential Equations*, *73*, 309–317.

Graham, M., & Kevrekidis, I. G. (1991). Alternative approaches to Karhunen–Loéve decomposition for model reduction and data analysis. *Computers in Chemical Engineering*, *20*, 1359–1374.

Holmes, P. J., Lumley, L., & Berkooz, G. (1997). *Turbulence, coherent structures, dynamical systems and symmetry*. New York, NY: Cambridge University Press.

Jolly, M. S., Kevrekidis, I. G., & Titi, E. S. (1990). Approximate inertial manifolds for the Kuramoto-Sivashinsky equation: Analysis and computation. *Physica D: Nonlinear Phenomena*, *44*, 36–47.

Khalil, H. K. (1996). *Nonlinear systems*. Upper Saddle River, NJ: Prentice-Hall.

Kuznetsov, Y. A. (1995). *Elements of applied bifurcation theory*. New York, NY: Springer.

Lall, S., Marsden, J. E., & Glavaski, S. (2002). A subspace approach to balanced truncation for model reduction of nonlinear control systems. *International Journal of Robust and Nonlinear Control*, *12*, 519–535.

Lorenz, E. N. (1956). *Empirical orthogonal functions and statistical weather prediction*. Technical report, Dept. of Meteorology Statistical Forecasting Project, MIT.

Mhaskar, P., Henson, M. A., & Hjortso, M. A. (2002). Cell population modeling and parameter estimation for continuous cultures of *Saccharomyces Cerevisiae. Biotechnological Progress*, *18*, 1010–1026.

Park, H. M., & Cho, D. H. (1996). The use of Karhunen-Loéve decomposition for the modeling of distributed parameter systems. *Chemical Engineering Science*, *51*, 81–98.

Parulekar, S. J., Semones, G. B., Rolf, M. J., Lievense, J. C., & Lim, H. C. (1986). Induction and elimination of oscillations in continuous cultures of *Saccharomyces Cerevisiae. Biotechnology and Bioengineering*, *28*, 700–710.

Porro, D. E., Martegani, B., Ranzi, M., & Alberghina, L. (1988). Oscillations in continuous cultures of budding yeasts: A segregated parameter analysis. *Biotechnology and Bioengineering*, *32*, 411–417.

Shvartsman, S. Y., & Kevrekidis, I. G. (1998). Nonlinear model reduction for control of distributed systems: A computer-assisted study. *A.I.Ch.E. Journal*, *44*, 1579–1595.

Sirovich, L. (1989). Low dimensional description of complicated phenomena. *Contemporary Mathematics*, *99*, 277–305.

Srienc, F., & Dien, B. S. (1992). Kinetics of the cell cycle of *Saccharomyces cerevisiae. Annuals of the New York Academy of Sciences*, *665*, 59–71.

Strassle, C., Sonnleitner, B., & Fiechter, A. (1988). A predictive model for the spontaneous synchronization of *Saccharomyces cerevisiae* grown in continuous culture. I. Concept. *Journal of Biotechnology*, *7*, 299–318.

Strassle, C., Sonnleitner, B., & Fiechter, A. (1989). A predictive model for the spontaneous synchronization of *Saccharomyces cerevisiae* grown in continuous culture. II. Experimental verification. *Journal of Biotechnology*, *9*, 191–208.

von Meyenburg, H. K. (1973). Stable synchrony oscillations in continuous culture of *Saccharomyces cerevisiae* under glucose limitation. In Chance, B., Pye, E. K., Shosh, A. K., & Hess, B. (Eds.), Biological and biochemical oscillators (pp. 411–417). New York, NY: Academic Press.

Zamamiri, A. M., Birol, G., & Hjortso, M. A. (2001). Multiple stable states and hysteresis in continuous, oscillating cultures of budding yeast. *Biotechnology and Bioengineering*, *75*, 305–312.

Zhang, Y., & Henson, M. A. (2001). Bifurcation analysis of continuous biochemical reactor models. *Biotechnological Progress*, *17*, 647–660.

Zhang, Y., Zamamiri, A. M., Henson, M. A., & Hjortso, M. A. (2002). Cell population models for bifurcation analysis and nonlinear control of continuous yeast bioreactors. *Journal of Process Control*, *12*, 721–734.

Zhu, G.-Y., Zamamiri, A. M., Henson, M. A., & Hjortso, M. A. (2000). Model predictive control of continuous yeast bioreactors using cell population models. *Chemical Engineering Science*, *55*, 6155–6167.